ALTISSIMO CONSULTING

Road Surface Noise

Exploration of the Influence of Surface Properties on Tyre/Road Noise

Client: NZ Transport Agency - Waka Kotahi
Date: 10th July 2024
Ref: 23-117-R05-C

Prepared for (the Client)
NZ Transport Agency – Waka Kotahi

Prepared by the Consultant)
Altissimo Consulting Ltd

Project	Road Surface Noise
Report	Exploration of the Influence of Surface Properties on Tyre/Road Noise
Reference	23-117-R05-C

Prepared by

George Bell
Consultant

Reviewed by

Robin Wareing
Principal Acoustic Engineer

Version history:

Version	Date	Comment
A	13-06-2024	Initial release for client review.
B	21-06-2024	Updated following client feedback.
C	10-07-2024	Updated following client feedback.

Report disclaimer and limitations:

This report has been prepared in accordance with the usual care and thoroughness of the consulting profession for the use of the Client. It is based on generally accepted practices and standards at the time it was prepared. No other warranty, expressed or implied, is made as to the professional advice included in this report.

This report should be read in full. No responsibility is accepted for use of any part of this report in any other context or for any other purpose or by third parties. This report does not purport to give legal advice. Legal advice can only be given by qualified legal practitioners.

Abstract

This investigation explored the influence of three road surface properties – thickness, mean profile depth (MPD), and void fraction – on the close proximity sound pressure level (L_{CPX}) across the Christchurch Northern Corridor (CNC), Christchurch Southern Motorway – Stage 2 (CSM2), and Peka Peka to Ōtaki Expressway (PP2Ō) projects.

Thickness was observed to be the dominant surface property influencing tyre/road noise, exhibiting a negative correlation with the overall L_{CPX} across all projects. The overall L_{CPX} was observed to be positively correlated with MPD. The greatest change in MPD occurred between porous asphalts with nominal maximum aggregate sizes of 7 and 10 mm. The overall L_{CPX} was observed to have a non-linear relationship with void fraction in the range of 5 to 22%, characterised by a local minimum at a void fraction of approximately 15%.

For the PA7, EPA7, and PA10 surfaces on CNC, lane 1 (right lane) was typically quieter than lane 2 (left lane) for the same thickness. This difference between lanes was explored further for the EPA7 (50 mm) surface for sections of road where the thickness was 50 ±3 mm. The spectrum for each lane indicated that the reduction in L_{CPX} between the lanes may arise from different acoustic absorption characteristics. It is recommended to directly test this hypothesis via absorption measurements.

The findings from this investigation reiterate the critical influence of thickness on tyre/road noise. In addition, changes in thickness, MPD, and void fraction explained the majority of the observed variation in L_{CPX}.

Contents

Glossary

CAPTIF	Canterbury Accelerated Pavement Testing Indoor Facility
CNC	Christchurch Northern Corridor
CPX	Close proximity
CPX laser	Laser line profile sensor installed on the CPX trailer
CSM2	Christchurch Southern Motorway – Stage 2
EPA	Epoxy modified porous asphalt
HSD	High speed data – an annual condition survey of the New Zealand state highway network
Lane 1	Closest lane to the centre of the road (see Figure 18)
Lane 2	Second-closest lane to the centre of the road (see Figure 18)
L_{CPX}	Close proximity sound pressure level. Shortened form of $L_{CPX:P1,80}$ (P1 tyre, 80 km/h reference speed)
LWP	Left wheel path
Macrotexture	The component of surface texture with wavelengths between 0.5 and 50 mm. Referred to as "texture" within this report.
MIT-SCAN	Brand of magnetic induction device used for point measurements of thickness.
MPD	Mean profile depth
NB	Northbound
NMAS	Nominal maximum aggregate size
OLS	Ordinary Least Squares
P1	Standard reference test tyre (passenger tyre)
PA	Porous asphalt
PA HS	Porous asphalt high strength
PA LV	Porous asphalt low voids
RMSE	Root mean square error
S2G	SH1 Johns Road from The Groynes to Sawyers Arms Road
SB	Southbound
SD	Standard deviation
SMA	Stone mastic asphalt
Thickness	Thickness of the top asphalt layer (i.e., wearing course)
VIF	Variance inflation factor
Void fraction	Sub-surface fraction of air within the asphalt
WBB	Western Belfast Bypass

1 Introduction

This investigation is a continuation of research into tyre/road noise led by Waka Kotahi (Noise and Vibration Research | Waka Kotahi NZ Transport Agency). The aim of this investigation was to expand upon the analyses of thickness, texture, and void fraction conducted in previous studies. This report is intended to be read in conjunction with the following documents:

- 22-104-R01-Road Noise Research - Analysis of asphaltic mix surfaces (Bell, 2023)
- 23-117-R01 – Road Surface Noise - Effects of porous asphalt thickness, ageing, and epoxy, and CPX speed and tyre hardness (Bell, 2024a)
- 23-117-R02 - Road Surface Noise - Influence of Void Fraction on Tyre-Road Noise (Bell, 2024b)
- 23-117-R03 - Road Surface Noise - Texture Measurement Validation and Its Effect on Tyre/Road Noise (Bell, 2024d)
- 23-117-R04 - Road Surface Noise - Measurement of the Acoustic Absorption of Asphaltic Mix Surfaces (Bell, 2024c)

Thickness was demonstrated to have a significant influence on the close proximity sound pressure level (L_{CPX}) through thickness trials on the Western Belfast Bypass (WBB) that was constructed in 2018 (Bull, 2019). The trial consisted of three approximately 300 m long sections of road with specified thicknesses of 30, 40, and 50 mm. The relationship was analysed using the mean L_{CPX} and specified thickness for each trial section (i.e., three samples). The relationship between L_{CPX} and thickness was explored further for CSM2 (Bell, 2023) and CNC (Bell, 2024a). The thickness in the left wheel path of lane 2 on CSM2 was measured using a precise level survey with a longitudinal resolution of approximately 3 m. The thickness on CNC was measured using a mobile laser survey (*Mobile Laser Scanning | Woods*, 2023) with a spatial resolution of 0.1 m and at points along the length using a MIT-SCAN device. Both investigations demonstrated that the overall L_{CPX} was negatively correlated with thickness. A preliminary analysis of the high-resolution data from CNC indicated the presence of complex relationships between L_{CPX} and thickness in the 630 to 2,500 Hz one third octave bands.

The relationships between L_{CPX} and macrotexture (hereafter "texture"), specifically MPD, were previously explored for CNC and S2G in (Bell, 2023); this study utilised a combination of texture measurements from the Road Science Hawkeye (*Hawkeye*, 2024) and annual high speed data (HSD) survey (WDM, 2019). In addition, multivariable regression was conducted with thickness for limited sections of CNC using the MIT-SCAN data. A positive correlation was observed between the overall L_{CPX} and MPD for the trial sections on S2G. The multivariable regression between L_{CPX}, thickness, and MPD for sections of CNC gave weak indications of positive correlations between L_{CPX} and MPD in the low frequency bands. Further analyses of texture using data collected by the CPX laser (Bell, 2024d) identified positive correlations between L_{CPX} and MPD in the low- to mid-frequency bands for porous asphaltic mixes; this analysis used univariate regression while limiting the range of thickness (e.g., 30 ±3 mm).

Void fraction was measured using a nuclear densometer (NDM) for a range of surfaces on CNC (Bell, 2024b). The overall L_{CPX} and void fraction were observed to be uncorrelated when considering all measurements. L_{CPX} and void fraction were observed to be negatively correlated in the 1,250 to 5,000 Hz bands.

The analyses within this report do not include the data from the acoustic absorption measurements on CNC (Bell, 2024c). However, the theoretical and observed absorption characteristics are referred to within the discussion of results.

The previous studies typically used univariate regression; with only a limited multivariable regression being undertaken. This investigation aimed to expand upon previous analyses through combining data from multiple projects, analysing targeted subsets, and performing univariate and multivariable regressions.

2 Data

This section contains summaries of the data used in the subsequent analyses. The section concludes with a summary of the range of each variable by project. All road segments used for the analyses had measurements of L_{CPX}, thickness, and MPD. Only a limited subset of segments on CNC had void fraction measurements.

2.1 Projects and Surfaces

Data from the Christchurch Northern Corridor (CNC), Christchurch Southern Motorway – Stage 2 (CSM2), and Peka Peka to Ōtaki Expressway (PP2Ō) projects were considered in this investigation. Thickness data were the limiting factor for not including a larger sample of projects as it cannot be determined retrospectively with sufficient accuracy and spatial resolution.

The lengths of road by lane, surface, and project are shown in Table 1. The lengths are of road segments that have L_{CPX}, thickness and MPD data. Only lane 2 of the southbound carriageway of PP2Ō was included in this investigation.

Table 1: Surfaces and lengths by project and lane.

Project	Surfacing Month(s)	Surface Type	Lane 2 km	Lane 1 km
CNC	Feb-Mar 2022	EPA7 (30 mm)	1.56	1.56
		EPA7 (50 mm)	4.61	4.61
		PA7 (30 mm)	5.09	5.09
		PA7 HS (30 mm)	0.35	0.35
		PA7 LV (30 mm)	0.39	0.39
		PA10 (30 mm)	0.38	0.38
CSM2	Apr 2021	EPA7 (40 mm)	2.85	-
PP2Ō	Nov 2022	EPA10 (25 mm)	4.98	-

2.2 Thickness

The longitudinal resolutions and method of thickness measurements by project are given in Table 2. Where multiple thickness measurements were present within a single CPX segment, the mean value was used. A core assumption of this investigation is that the method used to measure thickness does not influence the measurement itself (i.e., the laser survey, manual survey, and MIT-SCAN yield comparable results). This allows for direct comparison and correlation of thickness with tyre/road noise across the different projects. The thickness measurements by the mobile laser survey on CNC and manual precise level survey on CSM2 were comparable to measurements using MIT-SCAN disks on the same sites.

Table 2: Longitudinal spacing and measurement method for thickness by project.

Project	Method	Longitudinal Resolution	Carriageway	Lanes
CNC	Mobile laser survey	0.1 m	NB & SB	1 and 2
CSM2	Manual precise level survey	3 m	NB & SB	2
PP2Ō	MIT-SCAN disks	40 m	SB	2

The MIT-SCAN disks on PP2Ō were placed with a nominal longitudinal spacing of 40 m. The chainages were interpolated between known positions with a mean longitudinal spacing of 141 m. An accuracy of ±10 m was assumed for the longitudinal MIT-SCAN disk locations when expressed as chainages. The absence of individual GPS points for the locations for the majority of the MIT-SCAN disks represents a limitation for this investigation. The original purpose of installing the MIT-SCAN disks was not for road surface noise research and did not require high positional accuracy, for noise research purposes it is recommended that the locations of the MIT-SCAN disks are recorded using a high-accuracy GPS.

2.3 Tyre/Road Noise and Texture

Tyre/road noise and MPD were concurrently measured by the Waka Kotahi CPX trailer. All CPX measurements followed ISO 11819-2, are for the left wheel path (LWP) and were made with the P1 tyre at 80 km/h. The measurement dates and segment lengths are given for each project in Table 3. Longitudinal segments with a length of 20 m were used for PP2Ō to accommodate the assumed ±10 m accuracy of the interpolated MIT-SCAN disk locations. A data acquisition error invalidated the CPX laser texture measurements on PP2Ō; therefore, they were unable to be used in this investigation.

Table 3: Tyre/road noise and MPD measurement details.

Project	Lane	Measurement Date	Segment Lengths
CNC	1	03-06-2024	4 m
	2	04-01-2024	
CSM2	2	12-01-2024	4 m
PP2Ō	2	01-03-2024	20 m

2.4 Texture – HSD Survey

As usable MPD measurements from the CPX laser were not available for PP2Ō at the time of this investigation data from the 2024 HSD survey were used for the comparison of MPD between projects. It would have been preferable to use the MPD exclusively from the CPX laser. The survey date by location is given in Table 4. Where relative comparisons of MPD are made in the analyses, the data is always from the same source (i.e., CPX laser, or HSD survey). None of the analyses in this investigation attempted to correlate MPD from the HSD survey with L_{CPX}.

Table 4: HSD annual survey measurement dates by project.

Project	Measurement Date
CNC	01-03-2024
CSM2	02-03-2024
PP2Ō	18-11-2023

2.5 Void Fraction

Void fraction measurement data were available for CNC only. Measurements were undertaken on 28-11-2023, 20-02-2024, 21-02-2024 and covered a range of surface types and thicknesses. Most measurements were made in the left wheel path of lane 2, with a short section in lane 1 of the EPA7 (50 mm). 375-point measurements were made, corresponding to a total CPX segment length of 1.5 km (i.e. 375 x 4 m).

It is important to note that the void fraction data were not verified by volumetric measurements of core samples. The values must not be directly compared to the specified void fraction content in the mix designs.

2.6 Summary of Data

The total lengths of usable CPX segments by project with valid thickness, MPD, and void fraction data are given in Table 5. Thickness and MPD data were available for all CPX segments that contain void fraction.

Table 5: Total lengths of usable CPX segments by variable and project.

Project	Segment Length M	Thickness km	MPD* km	Void Fraction km
CNC	4	24.7	24.7	1.5
CSM2	4	2.9	2.9	-
PP2Ō	20	5.0	-	-

*Only includes CPX segments with valid thickness data and MPD values measured using the CPX laser.

Boxplots of L_{CPX}, thickness, MPD, and void fraction grouped by project are given in Figure 1.

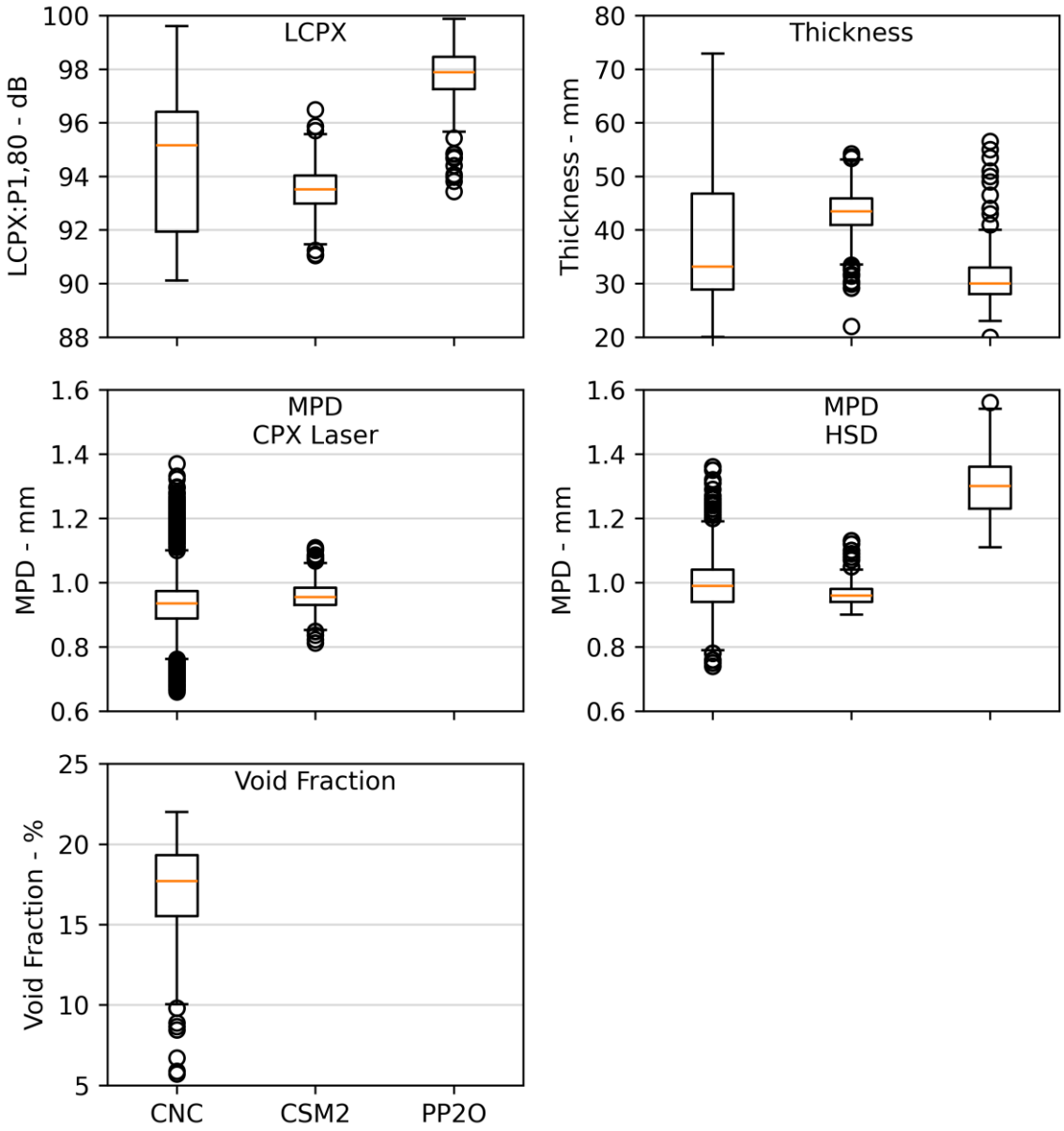

Figure 1: Boxplots of L_{CPX}, thickness, MPD (measured using the CPX laser), and void fraction grouped by project.

3 Analyses

The following analyses were conducted:

- Influence of thickness on:
  - Overall L_{CPX} for all data.
  - Overall L_{CPX} by lane and project for EPA7.
  - Overall L_{CPX} by lane and project for EPA10 and PA10.
  - Overall L_{CPX} by lane for EPA7 and PA7.
  - One-third octave bands for EPA7.
- Variation in MPD by project.
- Influence of void fraction on:
  - Overall L_{CPX} for a thickness of 30 ±3 mm.
  - One-third octave bands for a thickness of 30 ±3 mm.
- Comparison of L_{CPX} and MPD for lane 1 and 2 on CNC.
- Multivariable regression between L_{CPX} and thickness, MPD, and void fraction.

3.1 Thickness

This section presents univariate analyses exploring the relationships between tyre/road noise and thickness. Measured thickness data were available for the CNC, CSM2, and PP2Ō projects. The analyses first considered the overall relationship between L_{CPX} and thickness, then exploration of subsets of the data grouped by project, lane, NMAS, and epoxy presence. The section concludes with analyses of the relationships between each one-third octave band and thickness for the EPA7 on CNC.

3.1.1 Influence of Thickness on Overall L_{CPX}

Figure 2 shows the overall L_{CPX} versus thickness for all available data. A linear fit using the Ordinary Least Squares (OLS) method between L_{CPX} and thickness had a slope of -0.19 dB/mm, which corresponds to a decrease of 1.9 dB in L_{CPX} for an increase of 10 mm in thickness. Changes in thickness explained most of the observed variation in L_{CPX}, with the linear model achieving an R^2 of 0.70. However, the RMSE of the model was 1.2 dB, suggesting that while a significant portion of the variance was explained by the model, the unexplained variation still represents a meaningful range of noise levels.

Previous analyses have used linear (Bull, 2019), second-order polynomial (Bell, 2023), and fourth-order polynomial (Bell, 2024a) models. A linear fit was used here as a simple demonstration of the relationship. When a fourth-order polynomial was fitted to the data, the R^2 increased by 0.03 to 0.73, which suggests a linear fit explains a similar portion of the variability in this data to a fourth-order polynomial.

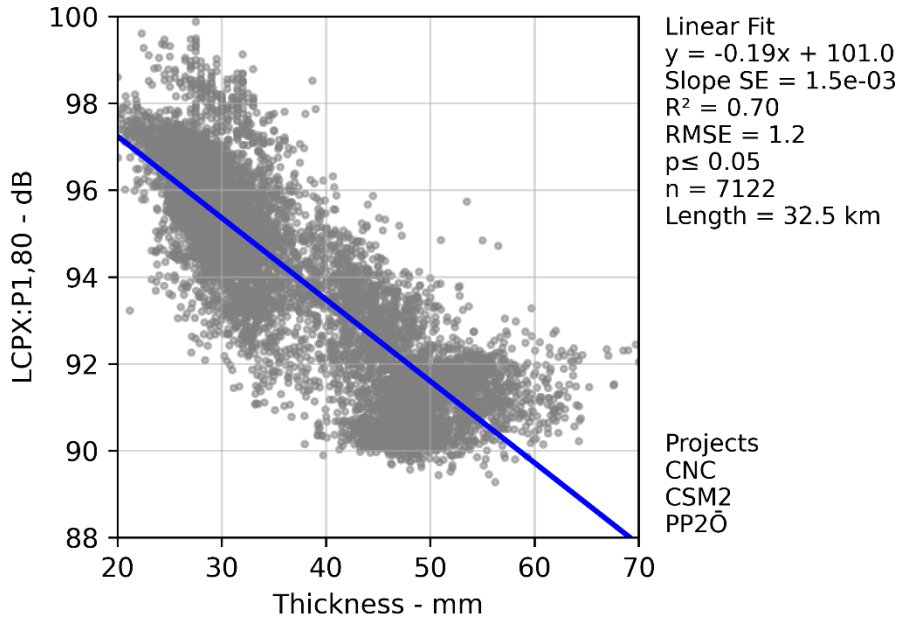

Figure 2: L_{CPX} versus thickness for all available data.

The following relationships between L_{CPX} and thickness utilise fourth-order polynomial models to capture possible non-linearities. Where models displayed signs of overfitting to the observed data the higher-order terms were sequentially removed. This process was continued until the majority of the remaining terms in each model achieved statistical significance ($p \leq 0.05$).

3.1.2 Influence of Thickness by Lane and Project for EPA7

The relationships between L_{CPX} and thickness were explored for epoxy modified porous asphaltic mixes with 7 mm NMAS by considering the following groups:

- EPA7, lane 2, CSM2
- EPA7, lane 2, CNC
- EPA7, lane 1, CNC

Equation 1 was fitted to each group of the observed data using the OLS method. The fitted models between L_{CPX} and thickness for each group are shown in Figure 3. The shaded area in Figure 3 represents the central 99% range of L_{CPX} for all thickness data (Figure 2). The coefficients for the fitted models are given in Table 6.

$$L_{CPX} = At^4 + Bt^3 + Ct^2 + Dt + J \qquad \text{Equation 1}$$

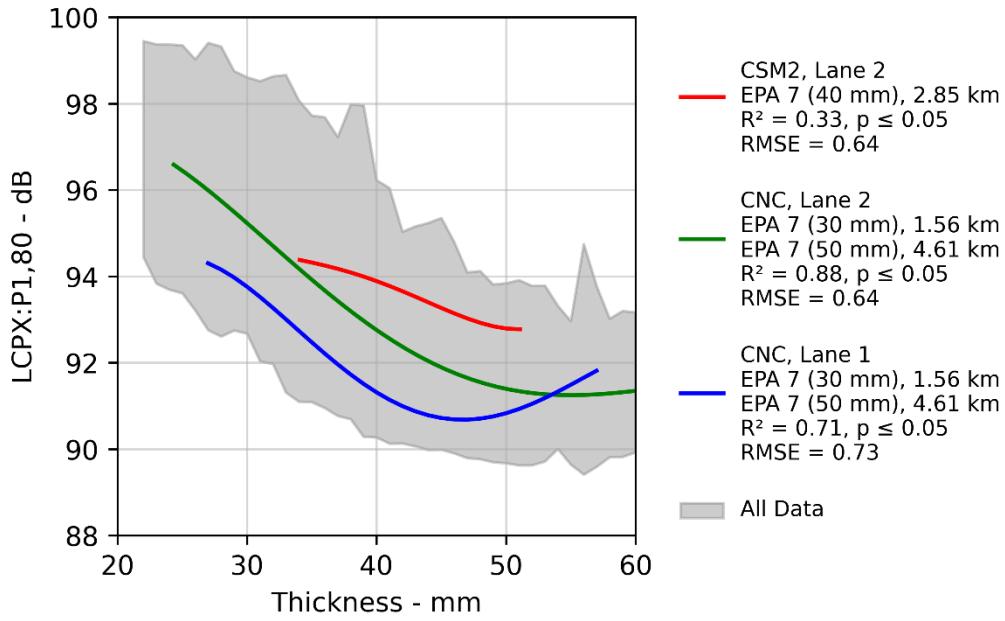

Figure 3: L_{CPX} versus thickness for EPA7 surfaces on CNC and CSM2.

The EPA7 in lane 2 on CSM2 (red line) had a higher L_{CPX} than its counterpart on CNC (green line) across the available range of thickness. L_{CPX} was influenced less by thickness in lane 2 of CSM2 compared to lane 2 of CNC. It is unknown whether this phenomenon is due to physical attributes of the surfaces or the reduced span of thickness for CSM2 compared to CNC.

For CNC, lane 1 of the EPA7 (blue line) had a lower L_{CPX} than lane 2 (green line) below a thickness of 54 mm. Lane 1 represents the majority of the lower bound of the full L_{CPX} versus thickness envelope. The mean difference between lane 1 and 2 on CNC was calculated for each 1 mm thickness band from 25 to 50 mm. A significant difference was present from 25 to 35 mm and 39 to 50 mm (t-test p-values ≤ 0.05). There were insufficient data to explore the differences in the 35 to 39 mm thickness range. The mean L_{CPX} was on average 1.5 dB less for lane 1 than lane 2.

The fourth-order polynomial models explained the majority of the observed variance in L_{CPX} for both lanes on CNC (green and blue lines), having R^2 values of 0.88 for lane 2 and 0.71 for lane 1. The model accounted for less of the observed variance in L_{CPX} for CSM2 (red line) with an R^2 of 0.33. The comparable RMSEs for all groups (0.64 to 0.73 dB) suggests that the resulting error in predictions is consistent across the three groups, despite the variations in R^2 values. This implies that, in terms of absolute error, the models perform similarly when explaining the observed variance in L_{CPX} within their respective groups.

3.1.3 Influence of Thickness by Lane and Project for EPA10 and PA10

The relationships between LCPX and thickness were explored for porous asphaltic mixes with 10 mm NMAS by considering the following groups:

- EPA10, lane 2, PP2Ō
- PA10, lane 2, CNC
- PA10, lane 1, CNC

Equation 1 was fitted to each group of the observed data using the OLS method. The fitted models between L_{CPX} and thickness for each group are shown in Figure 4. The shaded area in Figure 4 represents the central 99% range of L_{CPX} for all thickness data (Figure 2). The coefficients for the fitted models are given in Table 7.

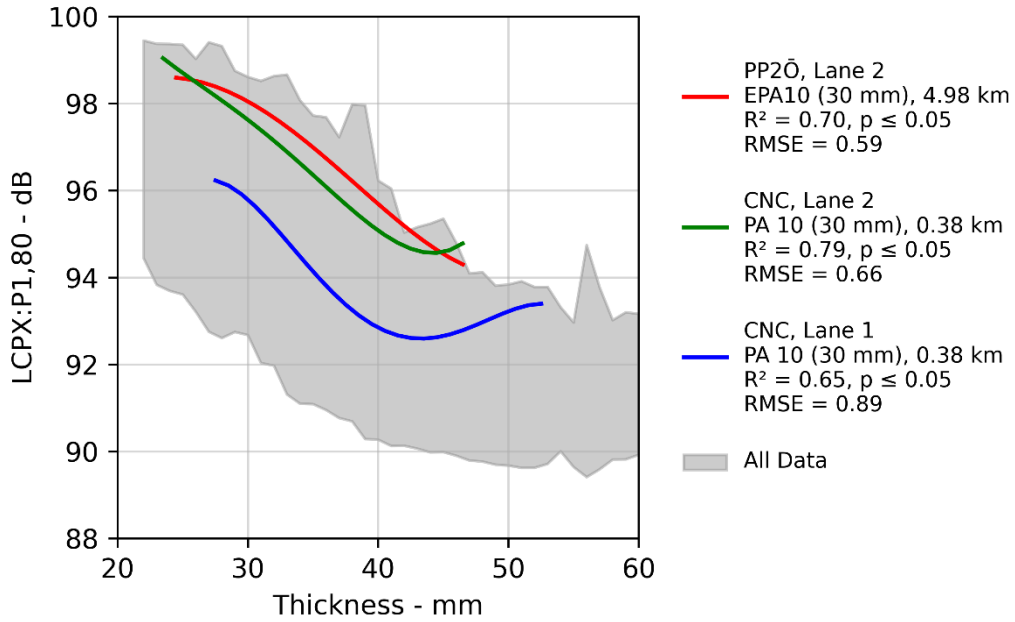

Figure 4: L_{CPX} versus thickness for EPA10 and PA10 surfaces on PP2Ō and CNC.

Lane 2 of the EPA10 on PP2Ō (red line) and PA10 on CNC (green line) had comparable fits between thicknesses of 25 and 40 mm. As observed in Figure 3 for the EPA7 on CNC, lane 1 of the PA10 on CNC (blue line) had a lower mean L_{CPX} than lane 2 (green line) across the available thickness span. The EPA10 and PA10 in lane 2 on CNC and PP2Ō represent the majority of the upper bound of the full L_{CPX} versus thickness envelope.

The mean difference between lane 1 and 2 of the PA10 on CNC was calculated for each 3 mm thickness band from 30 to 42 mm. A wider band was used than for the EPA7 due to the short sample length. It was assumed that the change in band width does not affect the analysis. A significant difference was present across the evaluated thickness range (t-test p-values ≤ 0.05). The mean L_{CPX} was on average 2.0 dB less for lane 1 than lane 2.

The fourth-order polynomial models explain most of the observed variance in L_{CPX} for all groups, having R^2 values of 0.65 to 0.79. The comparable RMSEs for all groups (0.59 to 0.89 dB) suggests that, in terms of absolute error, the models perform similarly when explaining the observed variance in L_{CPX} within their respective groups.

3.1.4 Influence of Thickness by Lane for EPA7 and PA7

The relationships between LCPX and thickness were explored for standard and epoxy modified porous asphaltic mixes by considering the following groups:

- PA7, lane 2, CNC
- PA7, lane 1, CNC
- EPA7, lane 2, CNC

Equation 1 was fitted to each group of the observed data using the OLS method. The fitted models between L_{CPX} and thickness for each lane of PA7 are shown in Figure 5 along with the fitted model for lane 2 of the EPA7 from Figure 3. The shaded area in Figure 5 represents the central 99% range of L_{CPX} for all thickness data (Figure 2). The coefficients for the fitted models are given in Table 6 and Table 8.

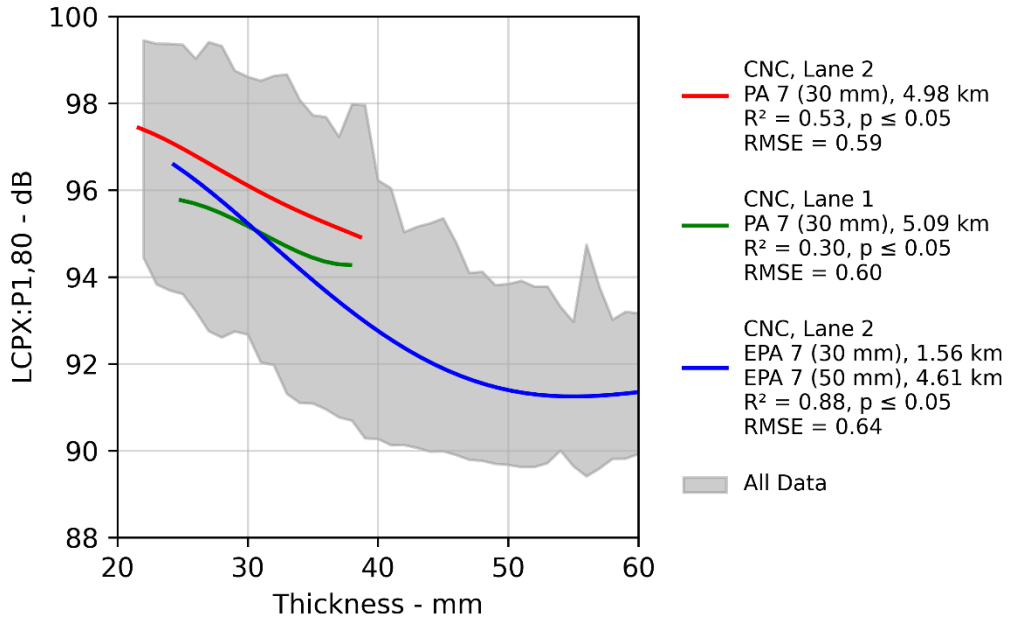

Figure 5: L_{CPX} versus thickness for EPA7 and PA7 mixes on CNC.

As observed above for the EPA7 and PA10, lane 1 of the PA7 on CNC (green line) had a lower mean L_{CPX} than lane 2 (red line) across the observed thickness span. Both lanes of the PA7 had elevated levels relative to their EPA7 counterparts. The rate-of-change of L_{CPX} with thickness of lane 2 of the PA7 (red line) was less steep than lane 2 of the EPA7 (blue line), meaning that the observed reduction in L_{CPX} for EPA7 over PA7 increased with increasing thickness. This trend cannot currently be extrapolated beyond a thickness of 38 mm due to the absence of data at greater thicknesses for PA7.

The fourth-order polynomial model explains the majority of the observed variance in L_{CPX} for lane 2 of the PA7 (green line), having an R^2 of 0.53. The model for lane 1 of the PA7 (green line) only explained a smaller proportion of the observed variance, having an R^2 of 0.30. However, the comparable RMSEs for both lanes of the PA7 (0.59 to 0.60 dB) suggests that, in terms of absolute error, the models perform similarly when explaining the observed variance in L_{CPX}.

3.1.5 Influence of Thickness on L_{CPX} by One-Third Octave Band

The relationships between each one-third octave band and thickness were explored for lane 2 of the EPA7 on CNC. This 6.17 km sample was selected as it had relatively large L_{CPX} and thickness spans. Equation 1 was fitted to the observed data using the OLS method. The fitted models demonstrated reasonable explanatory power (R^2 of 0.58 to 0.87) in the 630 to 2,000 Hz bands. The fitted models in the 315 to 500, and 2,500 to 5,000 Hz bands had poor explanatory power (R^2 of 0.05 to 0.23). The observed data and the fitted models for the 630 to 2,000 Hz bands are shown in Figure 6. The coefficients for the fitted models are given in Table 9.

For the 630, 800, and 1,000 Hz bands it appeared that L_{CPX} was simply negatively correlated with thickness. However, in the 1,250, 1,600, and 2,000 Hz bands a more complex relationship was observed. In the 1,250 Hz band, L_{CPX} had a local minimum between 35 and 40 mm; this local minimum in L_{CPX} appeared at lower thicknesses in the 1,600 and 2,000 Hz bands. There was an apparent local maximum in L_{CPX} in the 2,000 Hz band. The observed relationships are characteristic of the thickness-dependent acoustic absorption of porous surfaces (Bell, 2024c; Berengier et al., 1990); this has not been explicitly explored within this investigation.

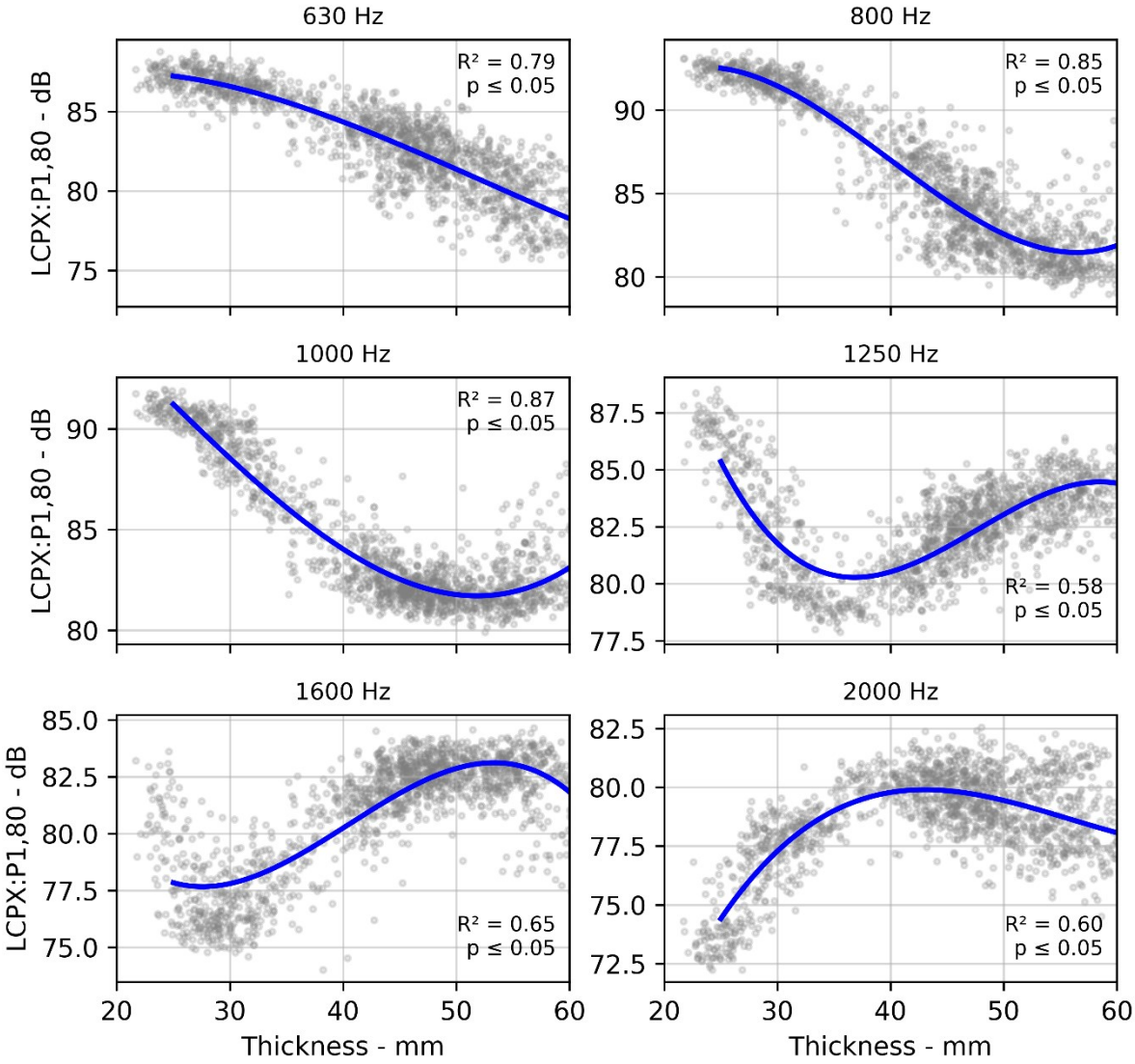

Figure 6: Observed data and fitted models for L_{CPX} and thickness for the 630 to 2,000 Hz bands for lane 2 of the EPA7 on CNC.

3.2 Mean Profile Depth

This section contains an analysis of the MPD collected during the 2024 HSD survey and is an expansion of the previous investigation on the influence of texture on tyre/road noise (Bell, 2024d). The HSD survey data were used to undertake comparisons of MPD for the same surface types on different projects. The HSD data were used because data from the CPX laser were not available for PP2Ō at the time of this analysis.

Figure 7 contains boxplots of the MPD from the HSD survey for lane 2 for the EPA7 surfaces on CNC and CSM2, and the EPA10 and PA10 surfaces on PP2Ō and CNC.

The mean MPD for the EPA7 on CSM2 was 0.02 mm greater than that on CNC. It is not expected that this observed difference in MPD has a significant influence on tyre/road noise. Both projects had the same mix design and were applied by the same contractor. At the time of measurement, the ages of the surfaces were 2.0 and 2.9 years for CNC and CSM2, respectively.

The mean MPD for the EPA10 on PP2Ō was 0.13 mm greater than the PA10 on CNC. The cause of the observed difference in MPDs is unknown. Key differences between the surfaces include (1) aggregate source, (2) use of epoxy, (3) underlying pavement (foam-bitumen stabilised for CNC and structural asphaltic concrete for PP2Ō), (4) and construction contractor. At the time of measurement, the ages of the surfaces were 1.0 and 2.0 years for PP2Ō and CNC, respectively.

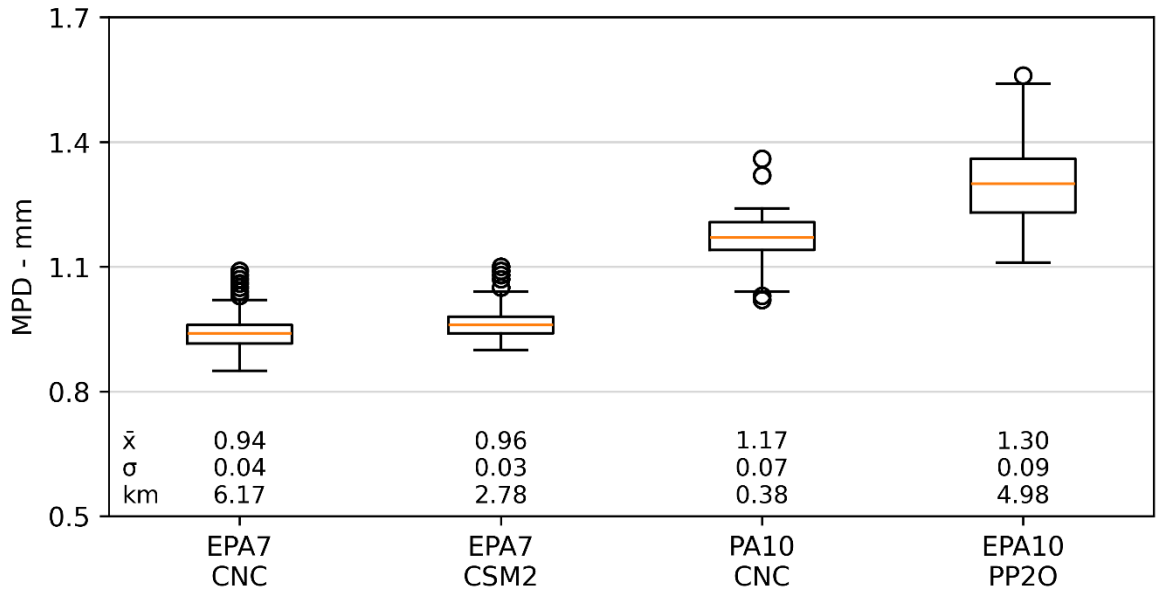

Figure 7: Boxplots of MPD from the 2024 HSD survey in lane 2 for porous asphaltic mixes grouped by project.

3.3 Void Fraction

This section contains analyses of the void fraction measured using the Road Science NDM and is an expansion of the previous investigation (Bell, 2024). Relationships between the overall and one-third octave bands were explored for a limited range of thickness.

3.3.1 Influence of Void Fraction for 30 mm Surfaces

The relationship between L_{CPX} and void fraction was explored by limiting the thickness to 30 ±3 mm (using the laser survey data from CNC). This filtering was applied to reduce the dominant influence of thickness on L_{CPX}; however, the remaining 6 mm range in thickness will still contribute to variance, particularly in locations with high void fraction (approximately greater than 15%). Equation 2 was fitted to the observed data using the OLS method. The observed data and the fitted model between L_{CPX} and void fraction are shown in Figure 8. The coefficients for the fitted model are given in Table 10.

$$L_{CPX} = Fv^4 + Gv^3 + Hv^2 + Iv + J \qquad \text{Equation 2}$$

The thickness was uniformly distributed from 27 to 33 mm (Chi Square Goodness of Fit Test $p > 0.05$). When the thickness was grouped into 2% wide void fraction bins, the mean value was 30 ±1 mm for all groups. The uniform distribution of thickness and absence of a significant relationship between thickness and void fraction indicates that the observed relationship between void fraction and L_{CPX} is not affected by thickness.

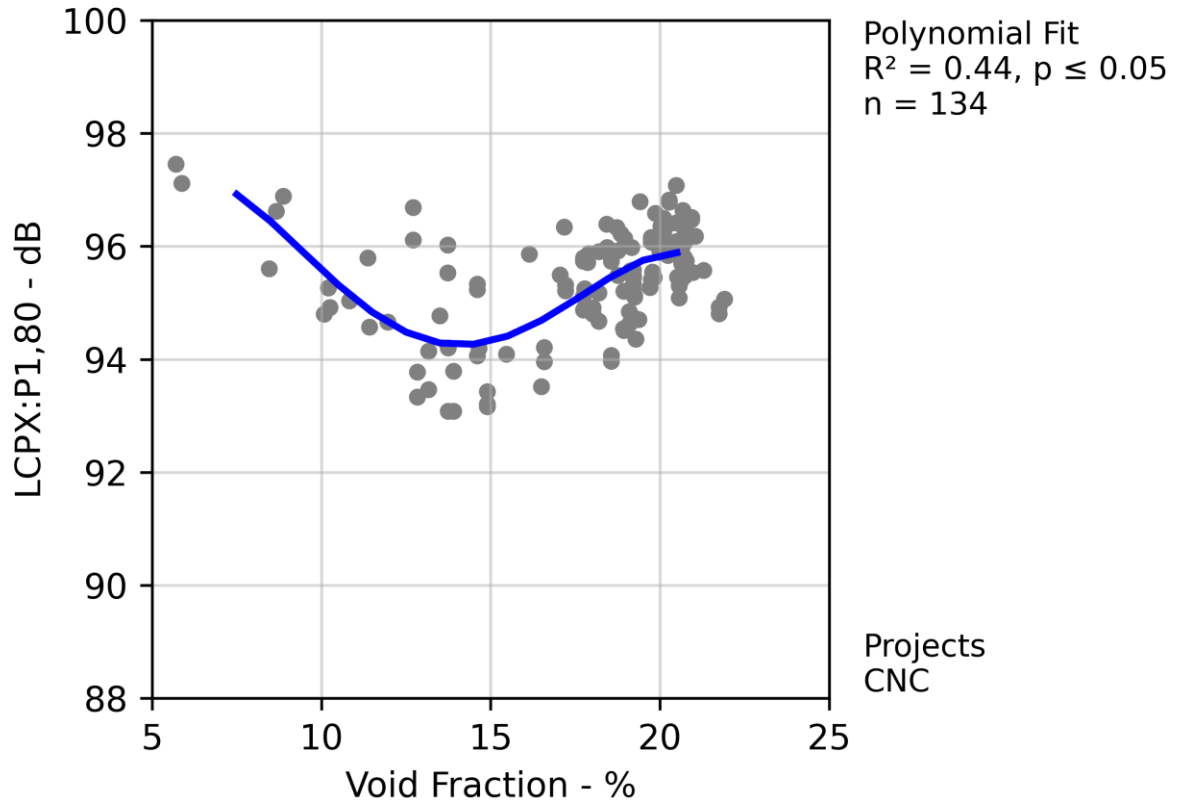

Figure 8: L_{CPX} versus void fraction for porous asphaltic mixes on CNC with thicknesses of 30 ±3 mm.

L_{CPX} decreased between void fractions of 5 to 15%, where it reached a local minimum, followed by an increase from 15 to 22%. The quantity of samples below a void fraction of 15% was very limited and therefore these observations must be considered as indicative. The fourth-order polynomial model explained a reasonable portion of the observed variance in L_{CPX}, having an R^2 value of 0.44.

3.3.2 Influence of Void Fraction on L_{CPX} by One-Third Octave Band

Linear fits were applied between each one-third octave band and void fraction for the 30 ±3 mm subset. The slopes of the linear fits and R^2 values with the observed data are given in Figure 9. Only significant relationships ($p \leq 0.05$) are shown. Void fraction was observed to be positively correlated with L_{CPX} in the 315 to 1,000 Hz bands and negatively correlated in the 1,250 to 5,000 Hz bands. The combination of the positive and negative correlations may explain the non-linear relationship observed above between the overall L_{CPX} and void fraction.

For the positively correlated bands, the 500 and 630 Hz bands were most influenced by perturbations in void fraction with slopes of approximately 0.4 dB/%. For the negatively correlated bands, the 1,600 and 2,000 Hz bands were most influenced by perturbations in void fraction with slopes less than -0.5 dB/%. It is hypothesised that the positive correlations are due to surface voids adding to texture and the subsequent increased excitation of the tyre. It is hypothesised that the negative correlations are due to a combination of reducing turbulent air flow noise through increased permeability and increasing acoustic absorption.

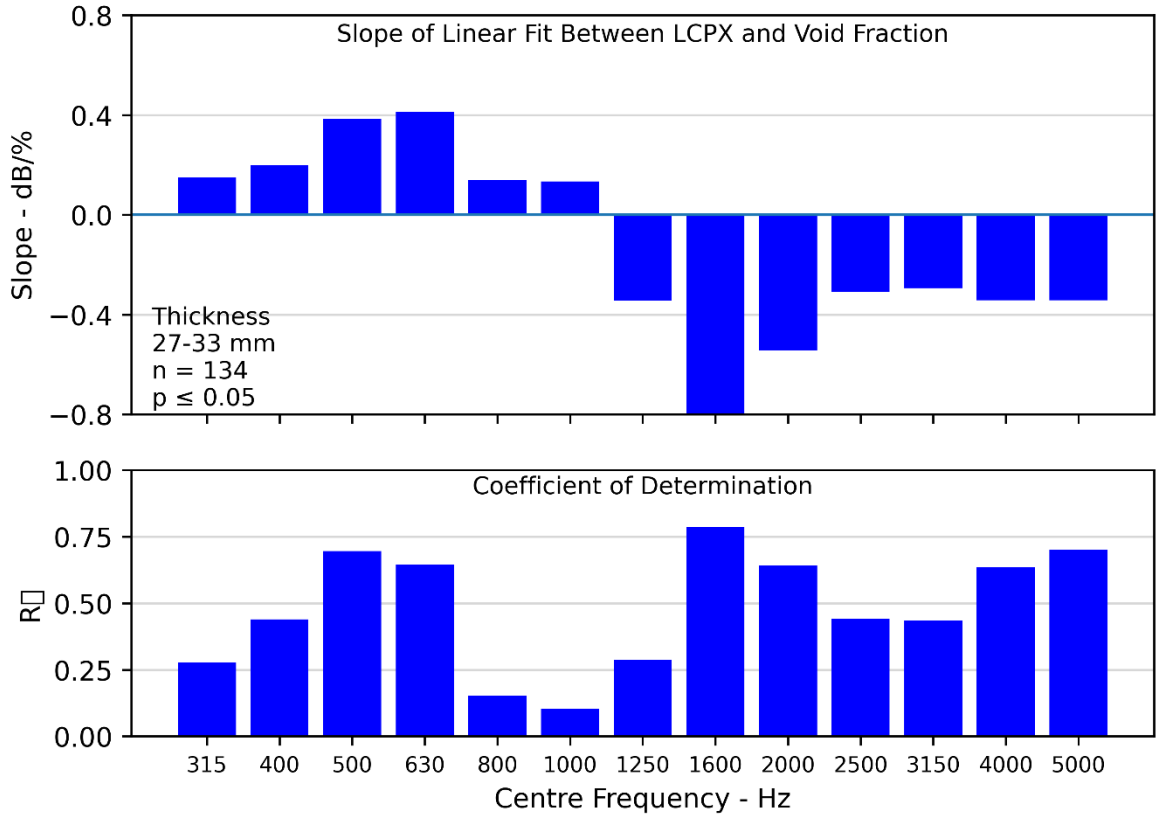

Figure 9: Slopes and R^2 values for each one-third octave band of linear fits between L_{CPX} and void fraction for porous asphaltic mixes on CNC with a thickness of 30 ±3 mm.

3.4 Changes between Lane 1 and Lane 2 on CNC

Analyses of the relationships between L_{CPX} and thickness presented in Section 3.1 identified that lane 1 was typically quieter than lane 2 for the same thickness. This phenomenon was explored further by exploring the differences in lane 1 and 2 of the EPA7 on CNC with thicknesses of 50 ±3 mm. Boxplots of the overall L_{CPX} and MPD from the CPX laser for each lane are shown in Figure 10. The mean difference in L_{CPX} between the lanes was 0.6 dB ($p \leq 0.05$). There was no physically significant difference between the mean MPDs of lanes 1 and 2.

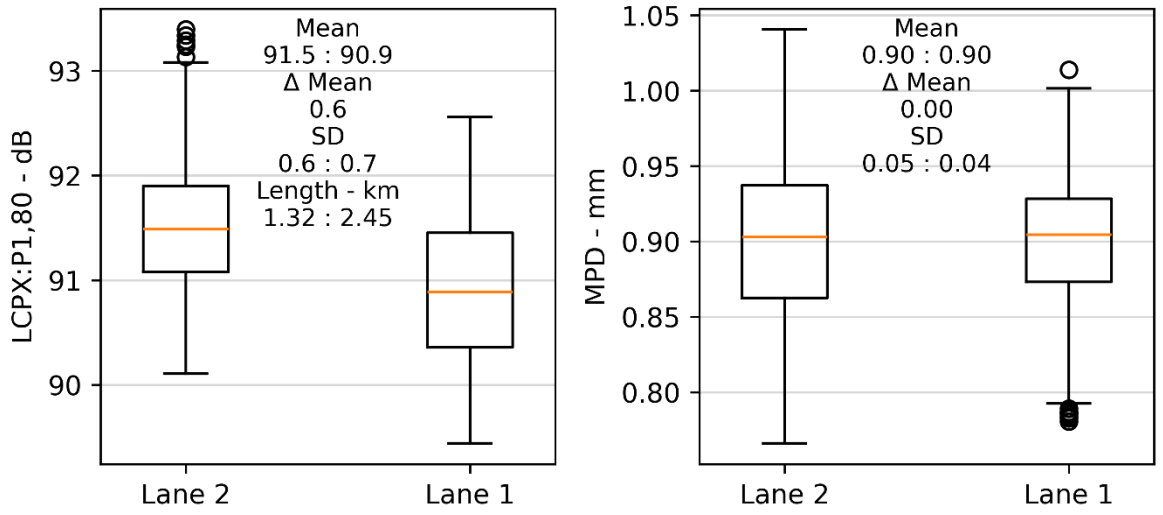

Figure 10: Boxplots of L_{CPX} and MPD from the CPX laser grouped by lane 1 and 2 for EPA7 (50 ±3 mm) on CNC.

The one-third octave band spectra for lane 1 and 2 and the difference (lane 1 minus lane 2) are shown in Figure 11. Lane 1 had lower levels in the 315 to 630, 1,600, and 2,000 Hz bands. The observed pattern in the differences may indicate a potential difference in absorption characteristics, specifically, a downward shift in the absorption peak frequencies for lane 1 relative to lane 2. It is recommended to measure the acoustic absorption to explore this hypothesis.

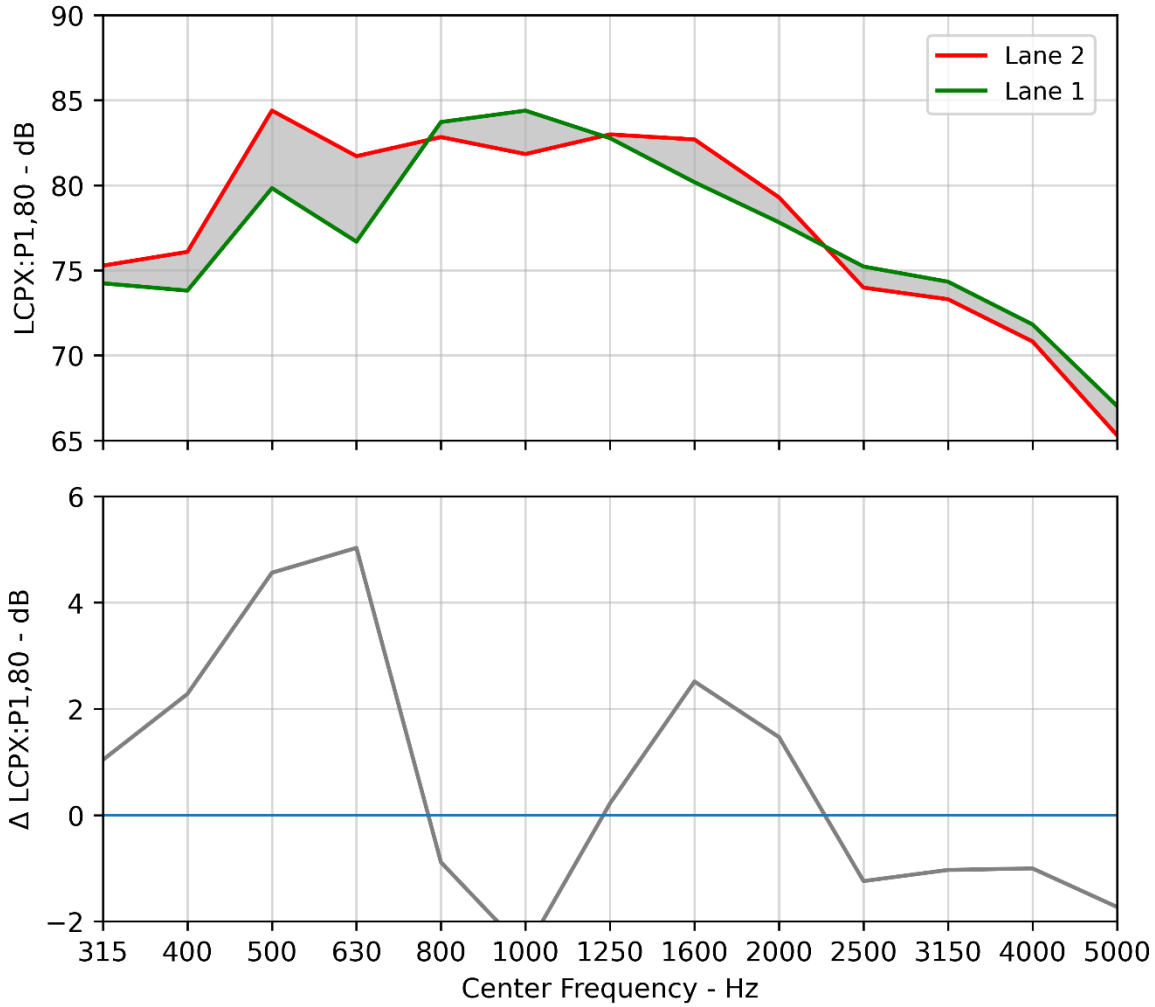

Figure 11: One-third octave band spectra grouped by lane 1 and 2 for EPA7 (50 ±3 mm) on CNC.

3.5 Multivariable Regression

Multivariable regression was used to explore the influence of thickness, MPD, and void fraction on both the overall and one-third octave band L_{CPX} for the porous asphaltic mix surfaces in lane 2 on CNC. The surfaces included EPA7 (30 mm), EPA7 (50 mm), PA7 (30 mm), PA7 HS (30 mm), and PA7 LV (30 mm). A total of 334 four-metre long CPX segments were used, having a total length of 1.34 km. Boxplots of L_{CPX}, thickness, MPD from the CPX laser, and void fraction for the data used in this analysis are given in Figure 12.

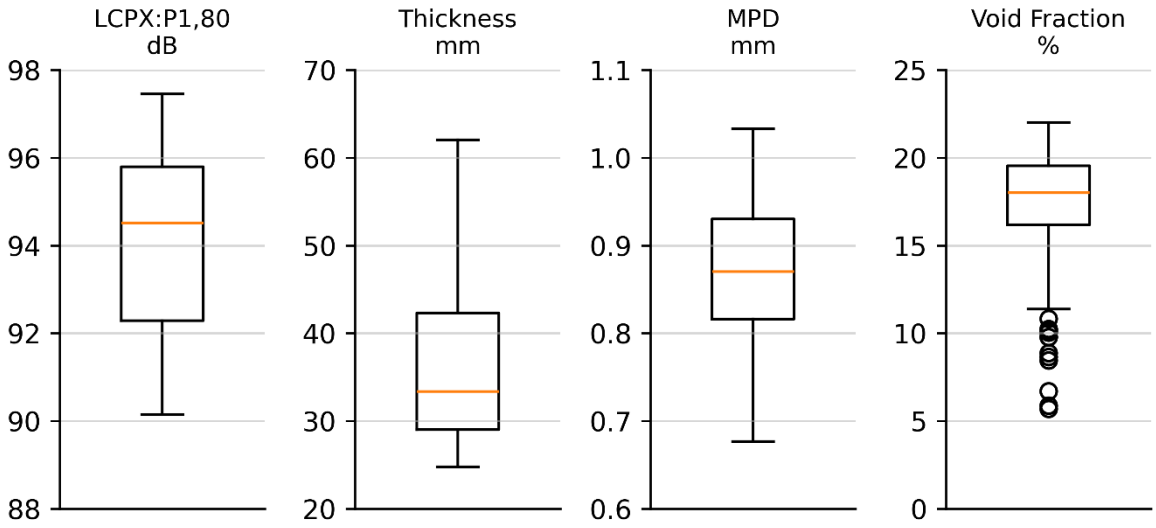

Figure 12: Boxplots of L_{CPX}, thickness, MPD from the CPX laser, and void fraction values for lane 2 of CNC.

It was identified in a previous investigation (Bell, 2024b) that void fraction and MPD were positively correlated. The presence of multicollinearity between independent variables must be considered for a multivariable analysis; this was assessed using the variance inflation factor (VIF). Within the data used in this analysis, thickness, MPD, and void fraction have VIFs of 1.1, 2.3, and 2.5, respectively. A general guideline for a VIF threshold where multicollinearity is considered to not significantly influence a regression model is a value less than three (*Variance Inflation Factor (VIF)*, 2023). As all of the VIFs are below three, thickness, MPD, and void fraction were considered as effectively independent variables.

Equation 3 was fitted to the observed data using the OLS method. The fitted model consisted of a fourth-order polynomial for thickness (t), a linear term for texture (m), and a fourth-order polynomial for void fraction (v). The coefficients for the fitted model are given in Table 11.

$$L_{CPX} = At^4 + Bt^3 + Ct^2 + Dt + Em + Fv^4 + Gv^3 + Hv^2 + Iv + J \quad \text{Equation 3}$$

The observed data and fitted model for L_{CPX} are shown in Figure 13 and Figure 14. The lines in the figures represent the fitted model. Within the plots, one independent variable is held constant, the next varied by three increments, and the last considered as a continuous variable (i.e., on the x axis). For example, the first plot in Figure 13 illustrates the model by holding the void fraction constant at 17.5%, while the MPD was set to 0.72, 0.87, and 1.02 mm, and the thickness was varied continuously from 25 to 60 mm. For MPD and void fraction, the three fixed values correspond to the mean, and the mean plus and minus two standard deviations. For thickness, nominal values of 30, 40, and 50 mm were used.

The model had excellent explanatory power for the observed variance in L_{CPX}, having an adjusted R^2 value of 0.89. L_{CPX} was negatively correlated with thickness across the included range. L_{CPX} was positively correlated with MPD, with the linear coefficient having a value of 6.76 dB/mm. The relationship between L_{CPX} and void fraction was non-linear, characterised by a local minimum at a void fraction of approximately 15%. The observed relationships are consistent between the multivariable and univariate analyses.

There were limited data for void fractions below 15%, therefore this relationship must be considered as indicative. In practice, the void fraction is either sufficiently high to be permeable to water or low so the surface acts as an impermeable barrier. Void fractions between 5 to 15% are not typically specified on New Zealand's highways. The standard porous asphaltic mixes (e.g., PA and EPA) had measured void fractions from 15 to 22%; over this range, the model attributes a 1 dB change in L_{CPX} due to void fraction.

For the observed data, the fitted model highlights that thickness was likely the dominant cause of variations in L_{CPX}.

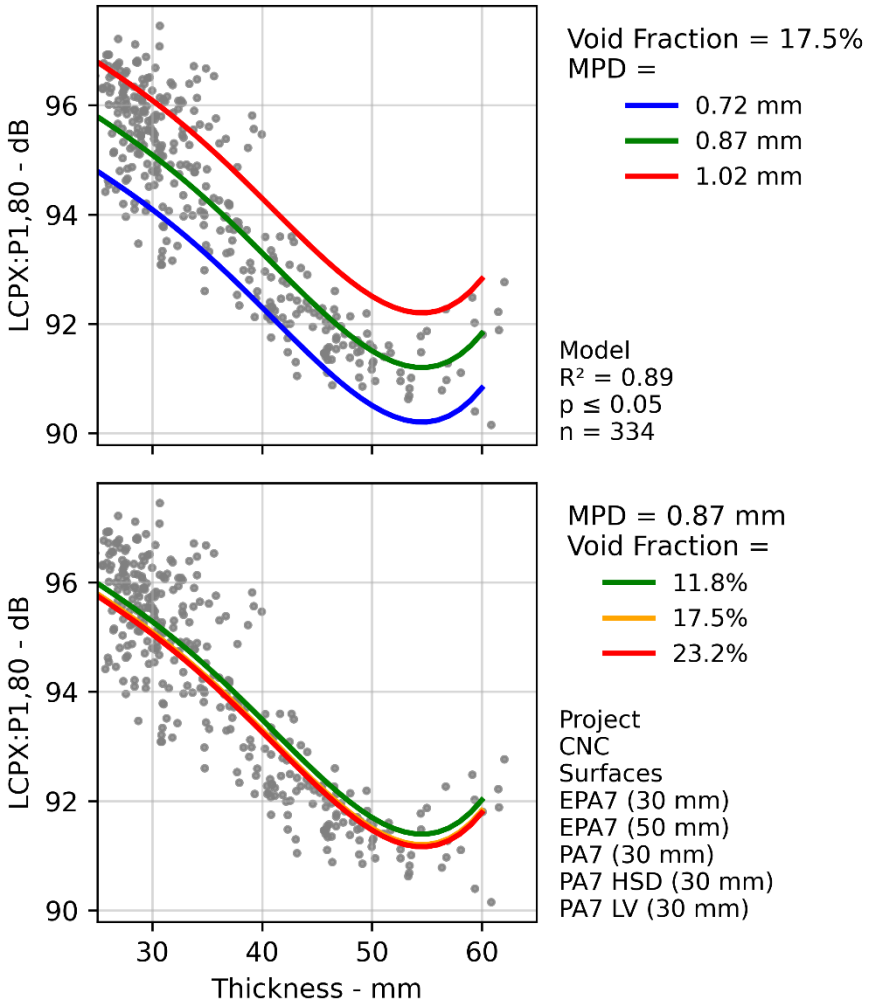

Figure 13: Observed data and fitted multivariable model for L_{CPX} and thickness, MPD, and void fraction.

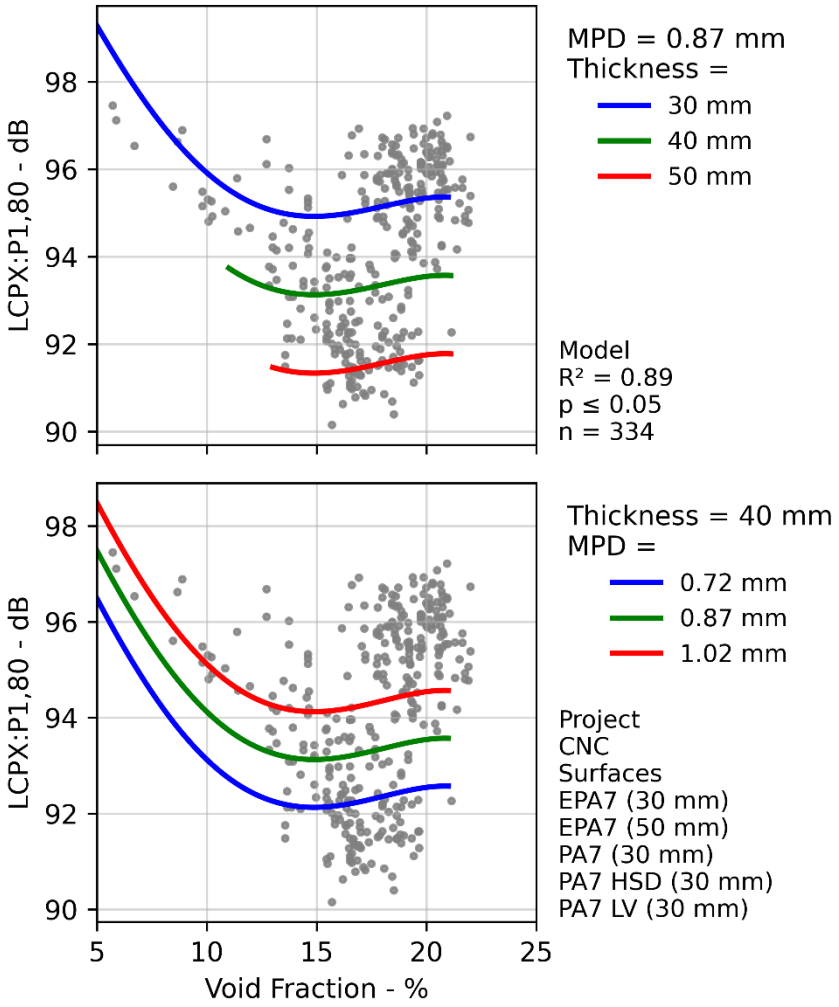

Figure 14: Observed data and fitted multivariable model for $L_{CPX\ and}$ thickness, MPD, and void fraction.

The relationships between L_{CPX} and thickness, MPD, and void fraction were explored for each one-third octave band. Equation 3 was fitted to the observed data using the OLS method. The coefficients of the second- to fourth-order void fraction terms were set to zero (i.e., using a linear model between L_{CPX} and void fraction). Linear models used in the univariate analysis between one-third octave bands and void fraction explained a reasonable portion of the observed variance (see Section 3.3.2).

The L_{CPX} spectra are shown in Figure 15 with the adjusted R^2 value for the fitted model in each frequency band. The grey area represents the central 95% range of L_{CPX} at each frequency.

The 630, 800, 1,000, and 1,600 Hz bands exhibited the greatest range; these bands coincided with those where the model had the highest explanatory power with all adjusted R^2 values being greater than 0.7. The models had moderate to strong explanatory power for the 500 to 2,000, 4,000, and 5,000 Hz bands. The models explained only a small portion of the observed variance in the 315, 400, 2500, and 3,150 Hz bands, which suggests that a surface property other than thickness, MPD, or void fraction is driving the observed variation.

The models demonstrated good explanatory power across the dominant frequency bands of the A-weighted spectrum, which is consistent with the good performance of the model in explaining the overall L_{CPX}.

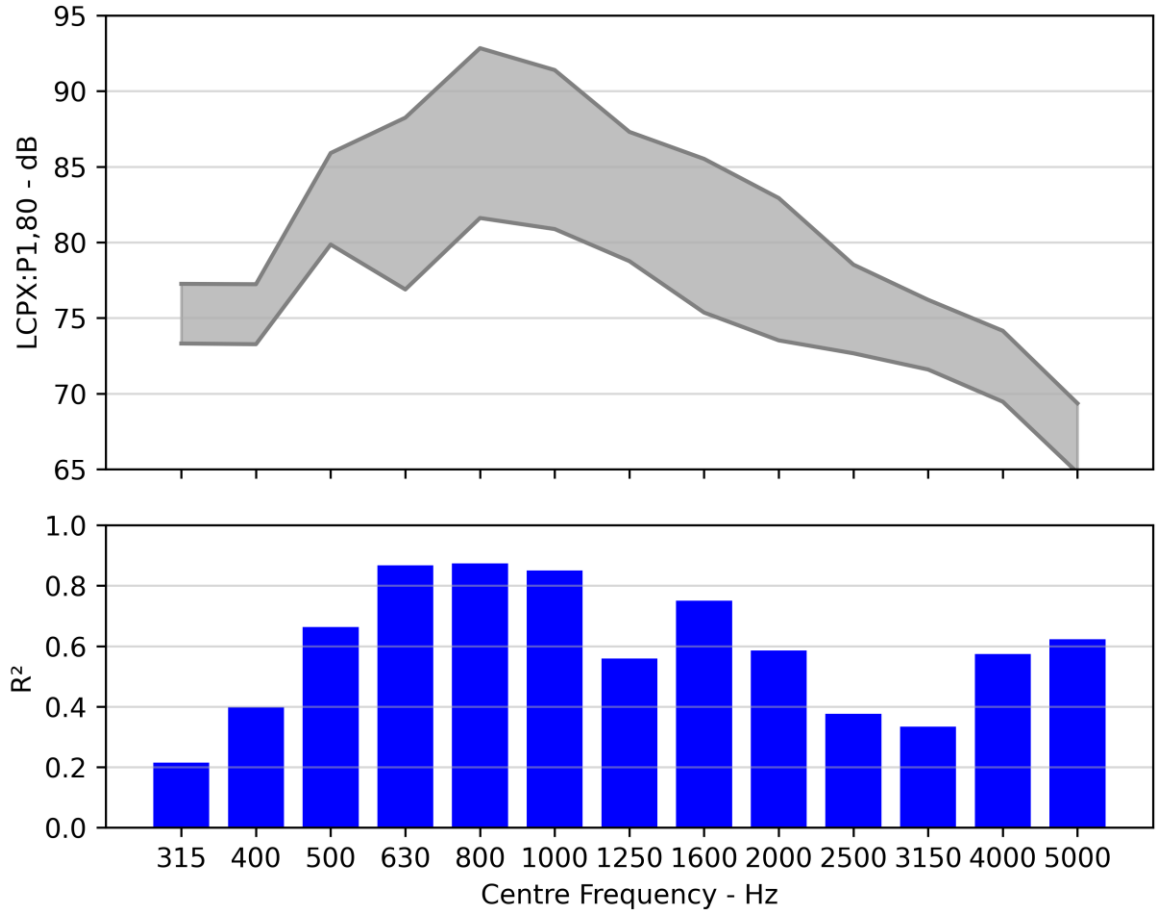

Figure 15: One-third octave band spectrum and range, and adjusted R^2 values of the fitted multivariable models.

The coefficients of the linear terms (i.e., slopes) for MPD and void fraction are shown by frequency band in Figure 16. Only values where $p \leq 0.05$ are shown. MPD was observed to be positively correlated with L_{CPX} in the 315 to 1,250 Hz bands, and negatively correlated in the 1,600, 2,000, 4,000, and 5,000 Hz bands. Void fraction was observed to be positively correlated with L_{CPX} in the 400 to 630 Hz bands, and negatively correlated in the 1,000 to 5,000 Hz bands. The observed correlations with void fraction are comparable to those observed in the univariate analyses (see Section 3.3.2), with key differences being the absences of positive correlations in the 315 and 800 Hz bands, and the reversal of the correlation in the 1,000 Hz band.

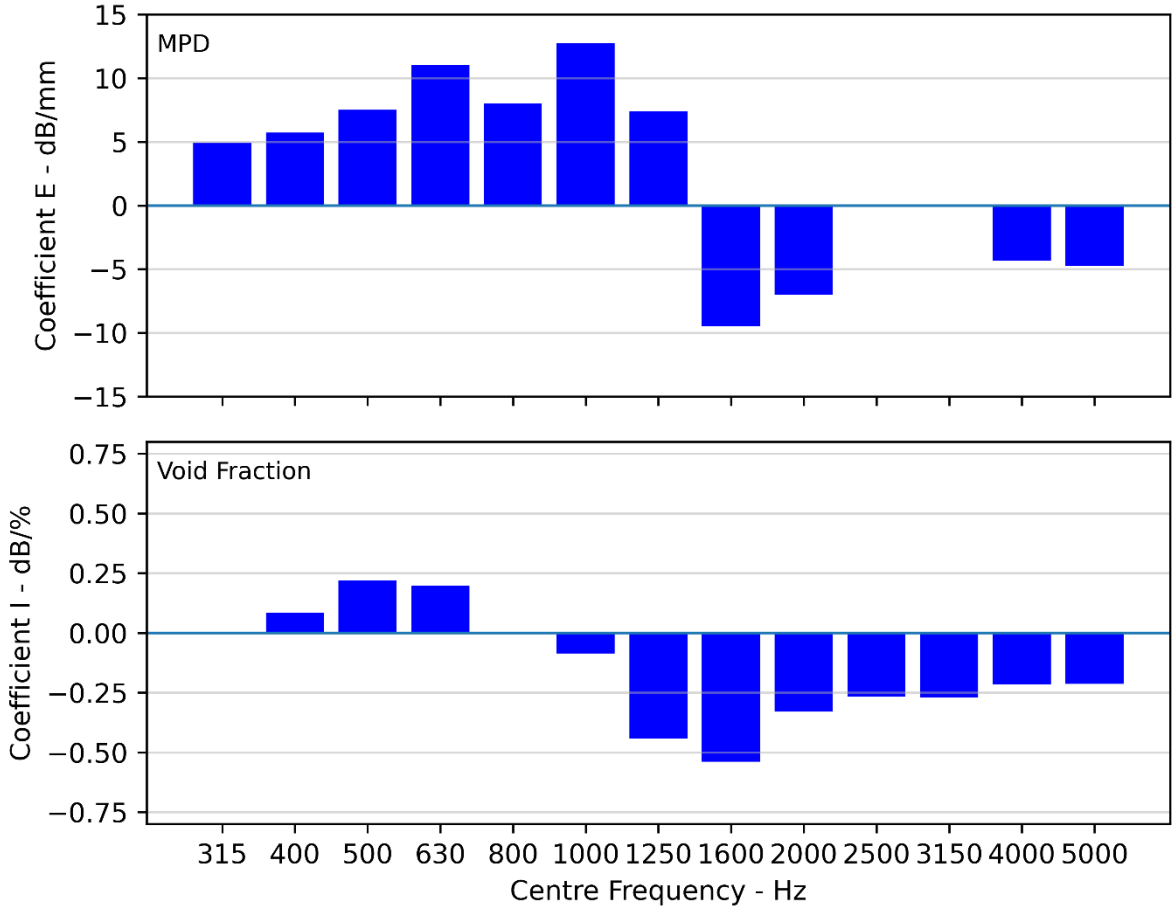

Figure 16: Coefficients of the linear terms for MPD and void fraction in the fitted multivariable models.

3.5.1 Illustration of the Influence of Thickness, MPD, and Void Fraction

For the data used in the multivariable regression, the observed overall L_{CPX} extended from approximately 90 to 97.5 dB. To illustrate the relative influence of each independent variable, the change in L_{CPX} was calculated using the fitted model (Table 11) and the 2.5th to the 97.5th percentile for thickness, MPD, and void fraction. The calculated change in L_{CPX} due to variations in each variable are shown in Figure 17. The largest calculated change in L_{CPX} was due to thickness, with the 26.0 to 57.7 mm span having a calculated change of 4.5 dB.

This illustration must not be interpreted as representing variations in L_{CPX} within a single surface specification. The data that were fitted to the model were from surfaces with:

- Specified thicknesses of 30 and 50 mm.
- Specified void fractions of 8 to 25%.

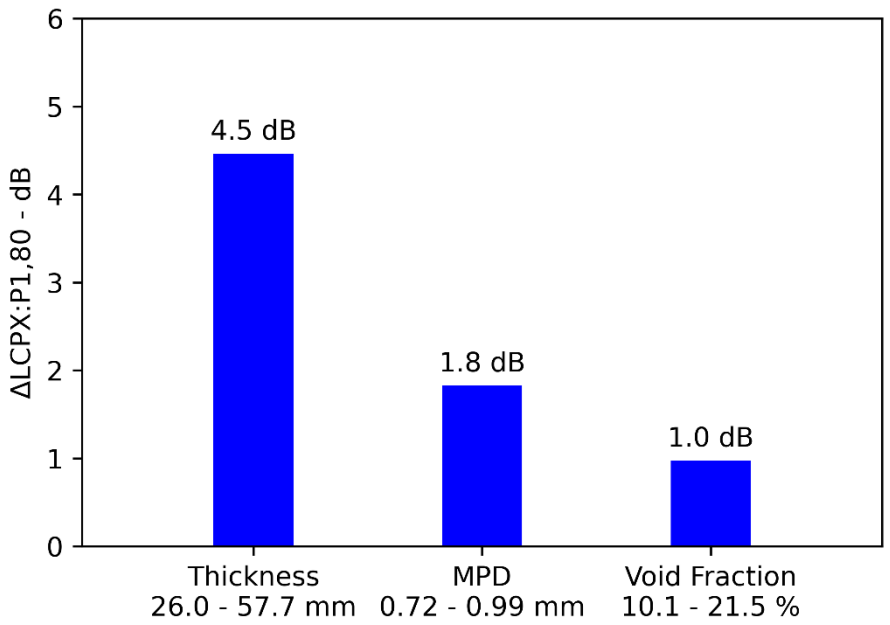

Figure 17: Calculated changes in L_{CPX} across the measured 2.5th to 97.5th percentiles of thickness, MPD, and void fraction.

4 Conclusions

As part of ongoing research led by Waka Kotahi, the influences of properties of porous asphaltic mix surfaces on tyre/road noise were explored across the CNC, CSM2, and PP2O projects. The surface properties that were considered included thickness, MPD, void fraction, NMAS, and the presence of epoxy in the binder. In addition, lane-to-lane, and project-to-project differences were explored. Both univariate and multivariable regression methods were used in the analyses. The analyses in this investigation expand on previous studies led by Waka Kotahi.

The overall L_{CPX} was observed to be negatively correlated with thickness across all projects. Complex relationships were observed between L_{CPX} and thickness in the 630 to 2,000 Hz one-third octave bands. The considered thickness range of approximately 20 to 65 mm accounted for the majority of the observed variation in L_{CPX}.

The overall L_{CPX} was observed to be positively correlated with MPD. The 315 to 1,250 Hz bands were positively correlated with MPD. The 1,600, 2,000, 4,000, and 5,000 Hz bands were negatively correlated with MPD.

A non-linear relationship was observed between L_{CPX} and void fraction, characterised by a local minimum at a void fraction of approximately 15%. L_{CPX} was observed to be positively correlated with void fraction in the 400 to 630 Hz bands and negatively correlated in the 1,000 to 5,000 Hz bands.

The differences between lanes 1 and 2 were investigated for the EPA7 (50 mm) surface on CNC. Lane 1 was on average 0.6 dB quieter than lane 2 for segments where the mean thickness was 50 ±3 mm. The differences in the differences in the L_{CPX} spectrum of each lane potentially indicate varying absorption characteristics; further absorption measurements are required to explore this hypothesis. The observed reduction in tyre/road noise from lane 2 to 1 represents a potential opportunity for further reductions without requiring an increase in thickness.

The observed relationships between L_{CPX} and thickness, MPD, and void fraction concur with findings from previous investigations led by the NZ Transport Agency – Waka Kotahi.

5 References

Bell, G. (2023). *Analysis of low-noise asphaltic mix surfaces: Texture, construction, and porosity effects*.

Bell, G. (2024a). *Effects of porous asphalt thickness, ageing, and epoxy, and CPX speed and tyre hardness* (23-117-R01; Road Surface Noise). Altissimo Consulting Limited.

Bell, G. (2024b). *Influence of Void Fraction on Tyre-Road Noise* (23-117-R02; Road Surface Noise). Altissimo Consulting Limited.

Bell, G. (2024c). *Measurement of the Acoustic Absorption of Asphaltic Mix Surfaces* (23-117-R04; Road Surface Noise). Altissimo Consulting Limited.

Bell, G. (2024d). *Texture Measurement Validation and Its Effect on Tyre/Road Noise* (23-117-R03; Road Surface Noise). Altissimo Consulting Limited.

Berengier, M., Hamet, J. F., & Bar, P. (1990). Acoustical Properties of Porous Asphalts: Theoretical and Environmental Aspects. *Transportation Research Record*, *1265*. https://trid.trb.org/view/348600

Bull, J. (2019). *Porous asphalt thickness and variability study*.

Hawkeye. (2024). Road Science. https://www.roadscience.co.nz/services/mobile-capture-data-collection/hawkeye

Mobile Laser Scanning | Woods. (2023, October 20). https://www.woods.co.nz/our-work/mobile-laser-scanning

Noise and vibration research | Waka Kotahi NZ Transport Agency. (n.d.). Retrieved January 25, 2024, from https://www.nzta.govt.nz/roads-and-rail/highways-information-portal/technical-disciplines/environment-and-sustainability-in-our-operations/environmental-technical-areas/noise-and-vibration/noise-and-vibration-research/#road-surface-noise-research

Variance Inflation Factor (VIF). (2023, September 30). Investopedia. https://www.investopedia.com/terms/v/variance-inflation-factor.asp

WDM. (2019). *High-speed data collection survey in NZ*. https://www.wdm.co.uk/news/on-the-road-again

Appendix A – Additional Data

Table 6: Coefficients for the fitted models in Figure 3.

Parameter	Coefficient	SE	P-value
CSM2, Lane 2, EPA7 (red line)			
A	2.91e-05	9.80e-06	≤ 0.05
B	-4.50e-03	1.54e-03	≤ 0.05
C	2.56e-01	8.91e-02	≤ 0.05
D	-6.43e+00	2.26e+00	≤ 0.05
J	1.55e+02	2.11e+01	≤ 0.05
CNC, Lane 2, EPA7 (green line)			
A	-5.73e-06	8.47e-07	≤ 0.05
B	1.07e-03	1.52e-04	≤ 0.05
C	-6.67e-02	1.00e-02	≤ 0.05
D	1.48e+00	2.84e-01	≤ 0.05
J	8.67e+01	2.93e+00	≤ 0.05
CNC, Lane 1, EPA7 (blue line)			
A	-1.97e-05	1.31e-06	≤ 0.05
B	3.54e-03	2.37e-04	≤ 0.05
C	-2.23e-01	1.57e-02	≤ 0.05
D	5.76e+00	4.51e-01	≤ 0.05
J	4.25e+01	4.74e+00	≤ 0.05

Table 7: Coefficients for the fitted models in Figure 4.

Parameter	Coefficient	SE	P-value
PP2Ō, Lane 2, EPA10 (red line)			
A	0	-	-
B	0	-	-
C	5.18e-04	7.48e-04	≤ 0.05
D	-2.05e-01	5.49e-02	≤ 0.05
J	1.04e+02	9.80e-01	≤ 0.05
CNC, Lane 2, PA10 (green line)			
A	0	-	-
B	0	-	-
C	3.50e-03	1.63e-03	≤ 0.05
D	-4.57e-01	1.15e-01	≤ 0.05
J	1.08e+02	2.00e+00	≤ 0.05
CNC, Lane 1, PA10 (blue line)			
A	0	-	-
B	0	-	-
C	1.20e-02	1.96e-03	≤ 0.05
D	-1.09e+00	1.54e-01	≤ 0.05
J	1.17e+02	2.95e+00	≤ 0.05

Table 8: Coefficients for the fitted models in Figure 5.

Parameter	Coefficient	SE	P-value
CNC, Lane 2, PA7 (red line)			
A	-2.30e-05	9.60e-06	≤ 0.05
B	2.99e-03	1.26e-03	≤ 0.05
C	-1.42e-01	6.10e-02	≤ 0.05
D	2.76e+00	1.29e+00	≤ 0.05
J	7.89e+01	9.99e+00	≤ 0.05
CNC, Lane 1, PA7 (green line)			
A	0	-	-
B	1.08e-03	1.72e-04	≤ 0.05
C	-9.95e-02	1.64e-02	≤ 0.05
D	2.90e+00	5.20e-01	≤ 0.05
J	6.87e+01	5.44e+00	≤ 0.05

Table 9: Coefficients of the fitted models for 630 to 2,000 Hz bands in Figure 6.

Parameter	Coefficient	SE	P-value
630 Hz			
A	0	-	-
B	9.99e-05	2.79e-05	≤ 0.05
C	-1.57e-02	3.70e-03	≤ 0.05
D	5.05e-01	1.58e-01	≤ 0.05
J	8.29e+01	2.15e+00	≤ 0.05
800 Hz			
A	-5.93e-06	2.17e-06	≤ 0.05
B	1.68e-03	3.90e-04	≤ 0.05
C	-1.44e-01	2.56e-02	≤ 0.05
D	4.40e+00	7.28e-01	≤ 0.05
J	4.81e+01	7.50e+00	≤ 0.05
1,000 Hz			
A	-1.77e-05	1.49e-06	≤ 0.05
B	3.39e-03	2.67e-04	≤ 0.05
C	-2.22e-01	1.76e-02	≤ 0.05
D	5.58e+00	4.99e-01	≤ 0.05
J	4.41e+01	5.14e+00	≤ 0.05
1,250 Hz			
A	1.47e-05	1.70e-06	≤ 0.05
B	-3.45e-03	3.06e-04	≤ 0.05
C	2.88e-01	2.01e-02	≤ 0.05
D	-1.01e+01	5.72e-01	≤ 0.05
J	2.05e+02	5.90e+00	≤ 0.05
1,600 Hz			
A	3.33e-05	1.77e-06	≤ 0.05
B	-6.61e-03	3.18e-04	≤ 0.05
C	4.66e-01	2.09e-02	≤ 0.05
D	-1.37e+01	5.94e-01	≤ 0.05
J	2.19e+02	6.13e+00	≤ 0.05
2,000 Hz			
A	0	-	-
B	3.01e-04	2.41e-05	≤ 0.05
C	-5.03e-02	3.20e-03	≤ 0.05
D	2.66e+00	1.36e-01	≤ 0.05
J	3.47e+01	1.86e+00	≤ 0.05

Table 10: Coefficients for the fitted model in Figure 8.

Parameter	Coefficient	SE	P-value
F	-8.39e-04	2.26e-04	≤ 0.05
G	4.56e-02	1.29e-02	≤ 0.05
H	-8.41e-01	2.65e-01	≤ 0.05
I	5.95e+00	2.29e+00	≤ 0.05
J	8.31e+01	6.94e+00	≤ 0.05

Table 11: Coefficients of the fitted multivariable model.

Parameter	Coefficient	SE	P-value
A	0	-	-
B	2.74e-04	4.28e-05	≤ 0.05
C	-3.17e-02	5.41e-03	≤ 0.05
D	1.02e+00	2.21e-01	≤ 0.05
E	6.76e+00	7.85e-01	≤ 0.05
F	0	-	-
G	-2.35e-03	6.25e-04	≤ 0.05
H	1.29e-01	2.77e-02	≤ 0.05
I	-2.29e+00	3.91e-01	≤ 0.05
J	9.29e+01	3.32e+00	≤ 0.05

Appendix B – Lane Labelling

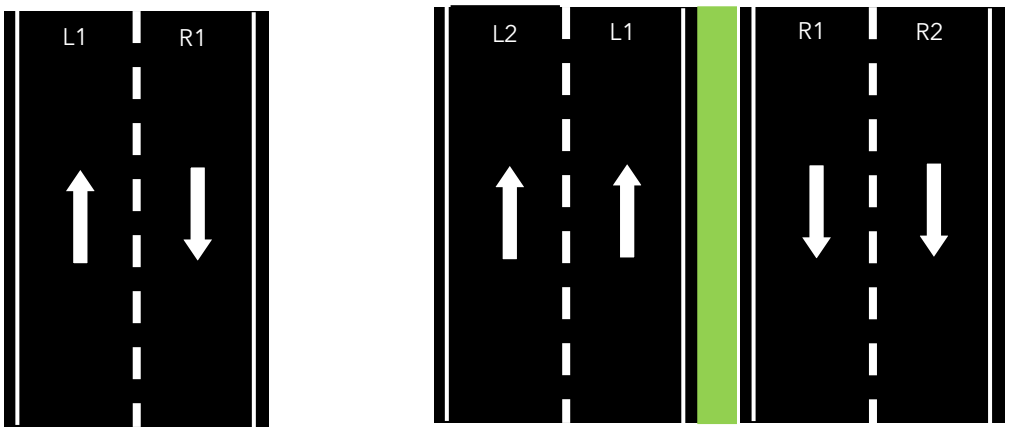

(a) Single carriageway (b) Dual carriageway

Figure 18. Lane labelling convention (assuming increasing direction toward the top of the page).